RSC Advances

PAPER

View Article Online
View Journal | View Issue

Cite this: *RSC Adv.*, 2026, **16**, 28131

Hemin–amino acid co-assembly nanozymes with dual enzyme-mimicking activities for *in situ* oxygen generation-enhanced one-step biosensing of glucose and H_2O_2

Yating Wang,†[ac] Yike Guo,†[a] Xiaofei Fu,†[a] Xuwen Li,[d] Yongri Jin,[d] Aifeng Wang,[ab] Yongcheng Ma[ab] and Ying Liu *[ab]

The co-assembly of amino acids or proteins with active small molecules to prepare biomimetic nanozymes offers a promising strategy for designing novel nanozymes. However, a significant challenge in nanozyme catalysis is the low activity at physiological pH, particularly for oxidase-like and peroxidase-like nanozymes. In this study, we successfully synthesized three biomimetic nanozymes (His@Hemin, Fe-His@Hemin, and Mn-His@Hemin) *via* the co-assembly of amphiphilic amino acids and hemin. Among these, the spherical Fe-His@Hemin exhibited superior peroxidase-like and catalase-like catalytic activities even in neutral pH systems. Free radical capture experiments revealed that Fe-His@Hemin, as a peroxidase-like nanozyme, generated three reactive oxygen species ($O_2^{\bullet-}$, $^1O_2$, and $^{\bullet}OH$), and as a catalase-like nanozyme produced oxygen during the catalytic process. This excellent catalase activity enabled *in situ* oxygen generation, which facilitated the oxidation of glucose oxidase within the system, providing a new strategy for one-step analysis of glucose and H_2O_2. The detection limits for glucose and H_2O_2 were as low as 0.25 μM and 0.16 μM, respectively, with linear ranges of 0.5–400 μM for glucose and 0.25–120 μM for H_2O_2. The glucose sensors demonstrated reliable and reproducible results for glucose determination in human serum.

Received 24th January 2026
Accepted 29th April 2026

DOI: 10.1039/d6ra00649c

rsc.li/rsc-advances

1 Introduction

Natural enzymes are mainly proteins with catalytic activity, which exist in organisms and nature, catalyze various biochemical reactions with high efficiency and specificity under mild conditions, and maintain the metabolism of organisms.[1–3] However, due to the high cost of natural enzymes, their variability and inactivation in non-mild environments, researchers have been constantly developing stable and high-performance artificial enzymes to make up for their disadvantages.[4–6] Nanozyme, as a kind of artificial enzyme, has been widely used in bioimaging, biochemical sensing, protein detection and biomedical therapy due to its excellent enzyme-like activity, high stability, flexibility in structural design and good biocompatibility.[7–10] In recent years, inspired by the active structure of horseradish peroxidase (HRP), biomimic nanozymes prepared by the co-assembly of amino acids or proteins with active small molecules provide a feasible strategy for the design of novel nanozymes.[11–15] Zhang's group[16] synthesized Hemin@BSA@ZIF-8 by encapsulating the hemin chloride/bovine serum albumin (BSA) co-assembly in zeolite imidazole ester skeleton structural material (ZIF-8). ZIF-8 encapsulation of Hemin@BSA not only improves the peroxidase activity of the biomimetic nanozyme, but also effectively prevents its decomposition or inactivation under harsh environments. Liu's group[17] mimicked the coordination structure of the metal porphyrin ring in natural peroxidase, and used metal–organic framework (MOF) material ZIF-8 as the precursor to design and synthesize a high-activity single atom nanozyme containing a Zn porphyrin structure. Through a series of experiments, it has been confirmed that the single atom Zn in the porphyrin structure of Zn is the key to its enzyme-like activity. However, most nanozymes display optimal catalytic activity exclusively within acidic to weakly acidic conditions; when the pH of the catalytic environment is increased to neutral (pH 7.0–8.0), the catalytic activity of the nanozymes decreases, which limits their application in the field of biological/chemical sensing.[18–20]

[a]*Department of Pharmacy, Fuwai Central China Cardiovascular Hospital, Zhengzhou, Henan 451464, China. E-mail: fwhzliuying@zzu.edu.cn*

[b]*Central China Subcenter of National Center for Cardiovascular Diseases, Henan Cardiovascular Disease Center, Fuwai Central-China Cardiovascular Hospital, Central China Fuwai Hospital of Zhengzhou University, Zhengzhou, Henan 450046, China*

[c]*School of Basic Medical Sciences, Zhengzhou University, Zhengzhou, Henan 450001, China*

[d]*College of Chemistry, Jilin University, Changchun, Jilin 130012, China*

† These authors contributed equally.

Glucose is our body's source of energy. The level of glucose in our blood is linked to our health. In the current glucose biosensors, the detection process of nanozymes is generally divided into two steps.[21–23] Firstly, Glucose oxidase (GOx) catalyzes to generate H_2O_2 in neutral buffer solution; secondly, peroxidase in acid buffer solution to induce color substrate to produce color signal. Yue's group[24] successfully detected glucose content in human blood using PtS_2 nanosheets at pH 5.0. Dong's group[25] synthesized 3D GH-5 nanoparticles and successfully established a glucose colorimetric sensor by a two-step method at pH 4.0. However, there are some defects in the practical operation and analytical performance of the two-step method for glucose detection. First, the pH of the reaction conditions in the first and second steps are different, which makes the actual operation process cumbersome. In addition, the reaction time is increased in the two-step method, which reduces the sensitivity of the detection system.[26–28] Therefore, the current strategy is to develop and design a novel nanozyme to detect glucose in a physiological environment by one-step method.

In this work, we successfully synthesized three biomimetic nanozymes (His@Hemin, Fe-His@Hemin, and Mn-His@Hemin) using an amphiphilic Fmoc-histidine and Heme co-assembly strategy. These nanozymes exhibit excellent peroxidase-like (POD-like) and catalase-like (CAT-like) activities and significantly broaden the pH working range of other nanozymes. Among them, Fe-His@Hemin demonstrates superior catalytic performance under physiological conditions. In glucose detection, the dual-enzyme characteristics of Fe-His@Hemin provide complementary advantages in the catalytic process. Specifically, its CAT-like activity catalyzes the conversion of H_2O_2 to O_2, and the *in situ* generated O_2 promotes the oxidation of glucose by GOx, thereby accelerating the reaction. As a result, the combination of Fe-His@Hemin and GOx establishes a one-step colorimetric method for glucose detection at physiological pH. This method is faster, simpler, and more sensitive than the traditional two-step approach. Additionally, this sensor has been successfully applied to glucose detection in both buffer solutions and human blood samples.

2 Materials and methods

2.1. Synthesis of His@Hemin

First, 24 μM Fmoc-histidine and 2.4 μM hemin were dissolved in 240 μL of DMSO. Then the above DMSO solution was added drop by drop to 5760 μL deionized water, stirred for 10 min. Next, the pH value of solution was adjusted to 7.0 with 1 M NaOH solution. Finally, the precipitation was collected by centrifugation and washed with water for 3 times.

2.2. Synthesis of Fe-His@Hemin

The preparation of Fe-His@Hemin was like that of His@Hemin synthesis. First, 24 μM Fmoc-histidine and 2.4 μM hemin were dissolved in 240 μL DMSO. Then the above DMSO solution was added drop by drop to 5760 μL $FeCl_3$ (24 μM) solution, stirred for 10 min. Next, the pH value of solution was adjusted to 7.0 with 1 M NaOH solution. Finally, the precipitation was collected by centrifugation and washed with water for 3 times.

2.3. Synthesis of Mn-His@Hemin

The preparation of Mn-His@Hemin was like that of His@Hemin synthesis. First, 24 μM Fmoc-histidine and 2.4 μM hemin were dissolved in 240 μL DMSO. Then the above DMSO solution was added drop by drop to 5760 μL $MnCl_2$ (24 μM) solution, stirred for 10 min. Next, the pH value of solution was adjusted to 7.0 with 1 M NaOH solution. Finally, the precipitation was collected by centrifugation and washed with water for 3 times.

3 Results and discussion

3.1. Construction and characterization of Fe-His@Hemin

Biomimic Fe-His@Hemin were synthesized by self-assembly using iron metal ions, amino acids and hemin. The transmission electron microscope (TEM) and scanning electron microscopy (SEM) image (Fig. 1a and b) shows the sphere morphology of Fe-His@Hemin had a relatively uniform spherical structure and the diameter of the particle was about 50–120 nm. The EDS mapping (Fig. 1c) clearly shows the presence of Fe, confirming that Fe is successfully incorporated into the nanozyme. The Powder X-ray Diffraction (PXRD) analysis provides crucial insights into the crystalline nature of materials (Fig. 1d). In this case, the absence of distinct diffraction peaks in the PXRD pattern suggests that the synthesized nanoparticles do not possess a long-range ordered crystal lattice structure. Instead, they exhibit an amorphous state, characterized by a disordered atomic arrangement. The Fourier transform infrared (FTIR) spectra (Fig. 1e) exhibit characteristic peaks at 1654 cm^{-1} (amide I, C=O stretching) and 1540 cm^{-1} (amide II, N–H bending) for both Fe-His@Hemin and His@Hemin, evidencing the successful co-assembly of Fmoc-histidine and hemin. Additional peaks at 1260 cm^{-1} (Fe–O) and 869 cm^{-1} (Fe–N) are observed in Fe-His@Hemin, further confirming Fe coordination. X-ray photoelectron spectroscopy (XPS) analysis was performed to study the elemental composition and surface oxidation states of Fe-His@Hemin. The survey spectrum (Fig. 2a–d) showed the Fe-His@Hemin has four elements, Fe, C, O, N. As shown in Fig. 2b, the binding energy of 713.7 eV corresponds to Fe $2p_{3/2}$ of Fe^{3+}, which is attributed to the presence of Fe^{3+} in Fe-His@Hemin. The peak at 724.6 eV is derived from Fe^{2+}, which may be due to the presence of a hemin active center of Fe^{2+}/Fe^{3+}. The binding energy of the N 1s spectrum (Fig. 2c) of Fe-His@Hemin at 399.1 eV is mainly related to Fe–N bonds.[29] The binding energy of C 1s (Fig. 2d) is located at 284.5 eV, which is mainly related to C–N. The hydrodynamic diameters of Fe-His@Hemin and His@Hemin were measured to be 110 ± 12 nm and 95 ± 10 nm, respectively, in PBS (pH = 8.0) (Fig. S1 and S2). Both samples exhibited excellent colloidal stability, with polydispersity indices (PDI) remaining below 0.18 in PBS (pH = 8.0). Furthermore, no aggregation was observed over a 24-hour incubation period at 25 °C. The content of iron in the inductively coupled plasma optical emission spectrometry (ICP-OES) test Fe-His@Hemin

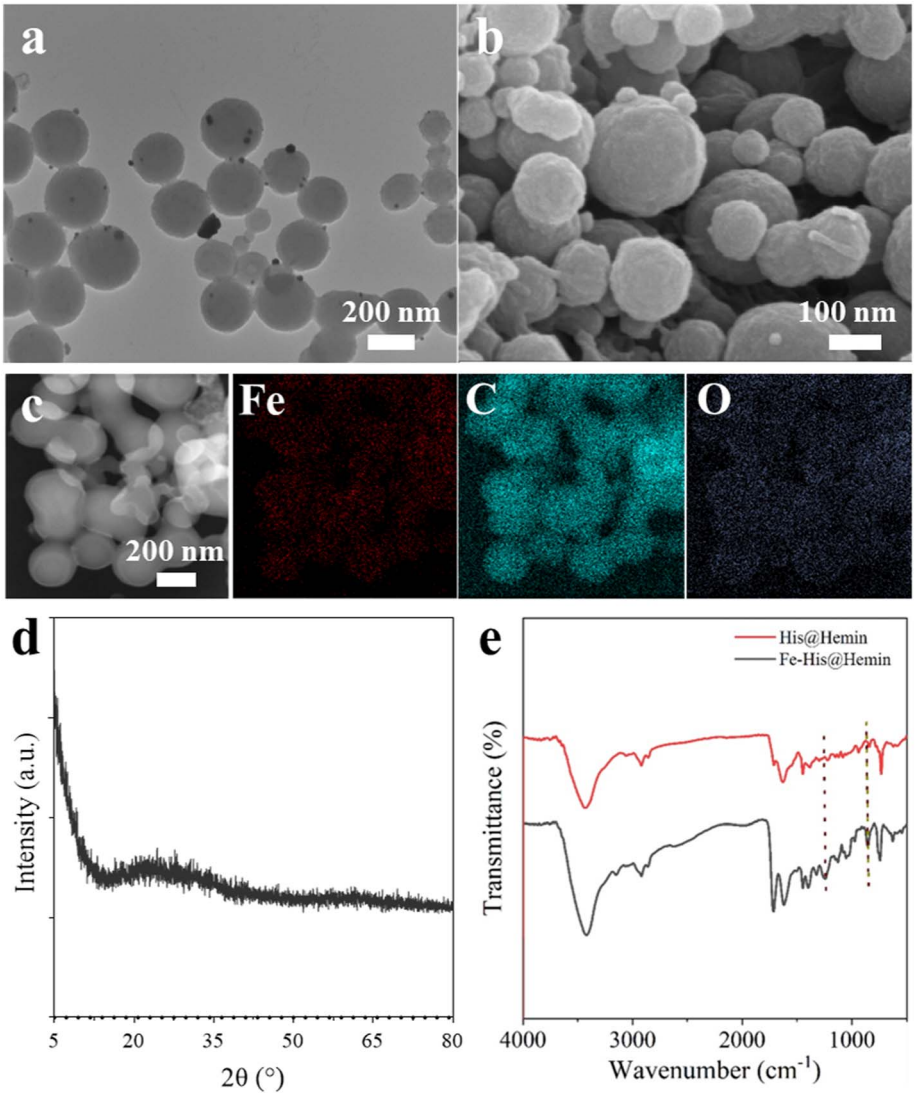

Fig. 1 Characterization of Fe-His@Hemin nanozymes. TEM (a), SEM (b) and EDS mapping (c) image of Fe-His@Hemin (d) the PXRD characterization of Fe-His@Hemin nanozymes (e) FTIR spectra of His@Hemin and Fe-His@Hemin.

was 0.49 ± 0.03 mg per g composite, which was greater than the content of iron in hemin and His@Hemin (0.22 ± 0.02 mg pre g composite), indicating that there were two forms of Fe in the biomimetic nanozyme: iron in hemin and exogenous Fe^{3+}.

3.2. Peroxidase-like activity of Fe-His@Hemin

The peroxidase-like activity of Fe-His@Hemin was investigated using several typical substrates, including TMB, OPD, and ABTS. In the presence of H_2O_2, these colorless substrates were oxidized to form colored products, confirming the peroxidase-like activity of Fe-His@Hemin (Fig. 3a). Among these substrates, TMB was selected for further experiments due to its optimal color development time, better linearity, higher sensitivity, and stability of the chromogenic product under the experimental conditions. Fig. 3b demonstrates that in the absence of H_2O_2, Fe-His@Hemin alone could not oxidize TMB without H_2O_2, which indicates that Fe-His@Hemin plays the role of a peroxidase-like mimic in the catalytic reaction between TMB and H_2O_2.

To evaluate the peroxide-like activities of Fe-His@Hemin, we compared the enzyme-like activities of hemin nanomaterials with different metals (Mn-His@Hemin and His@Hemin) (Fig. S3). When hemin was loaded with histidine, the absorbance was lower. However, the absorbance increased significantly when metal ions were continued to be loaded, among which Fe-His@Hemin had the highest catalytic activity. To support our claim regarding the superior catalytic activity of Fe-His@Hemin over Mn-His@Hemin, the morphology of Mn-His@Hemin was characterized by TEM (Fig. S7). The image reveals that Mn-His@Hemin exhibits a nanoparticulate aggregate structure with particle sizes ranging from approximately 80 to 150 nm, which is larger and more aggregated compared to the smaller, more dispersed Fe-His@Hemin nanoparticles. This morphological difference likely contributes to a reduced

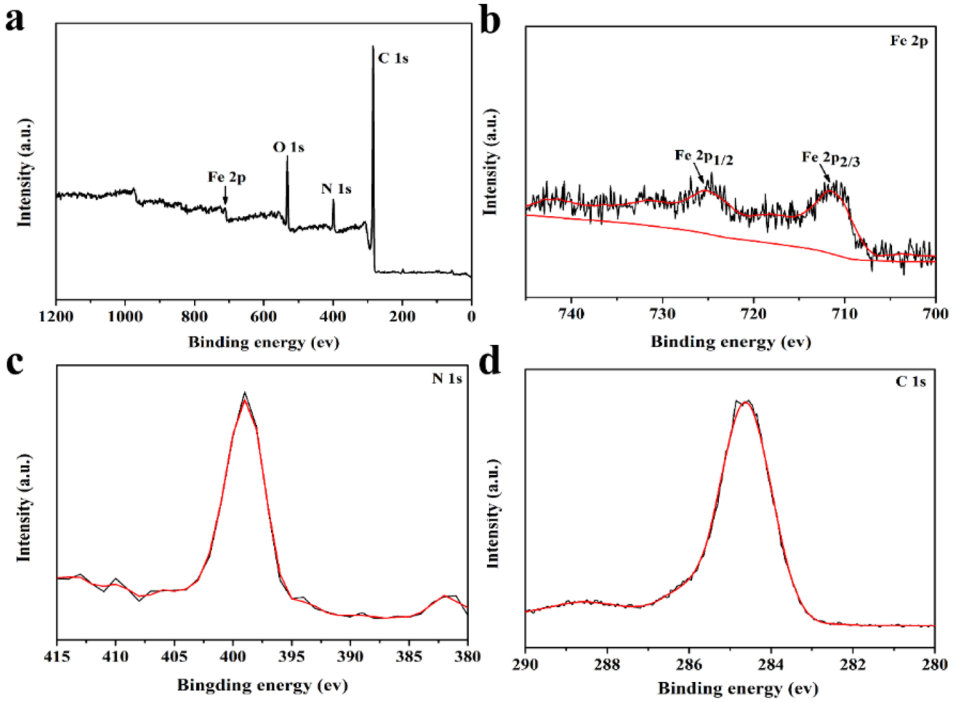

Fig. 2 Element and valence state analysis of Fe-His@Hemin. (a) XPS survey spectrum. High-resolution XPS spectra of the (b) Fe 2p, (c) N 1s, (d) C 1s for Fe-His@Hemin.

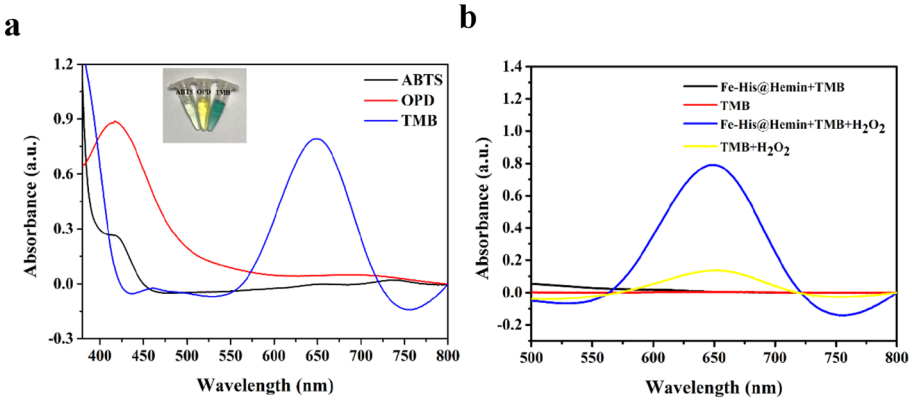

Fig. 3 Investigate the peroxidase-like activity of Fe-His@Hemin. (a) UV-vis spectra of ABTS, OPD, and TMB oxidized byFe-His@Hemin (Inset: photographs of the oxidation reaction of ABTS, OPD and TMB by Fe-His@Hemin). (b) Typical absorption spectra of TMB, TMB + H_2O_2, TMB + Fe-His@Hemin, TMB + H_2O_2+ Fe-His@Hemin at 652 nm (conditions: 0.3 mM TMB, 6 μg per mL Fe-His@Hemin, 0.1 M Tris–HCl buffer pH 8.0, 10 min and 25 °C).

accessible surface area for substrate binding and electron transfer in Mn-His@Hemin, thereby rationalizing its lower peroxidase-like activity. This indicated that the introduction of metal ions enhanced the enzyme-like catalytic activity of nanomaterials. Furthermore, the 3D microsphere structure of Fe-His@Hemin increased the effective catalytic sites, thus improving the catalytic activity of nanozyme. Like the properties of horseradish peroxidase (HRP), the peroxidase-like properties of Fe-His@Hemin depend on pH, temperature, H_2O_2 concentration, and the usage of nanozyme. As shown in Fig. 4a, the pH range of the three nanozymes is 3–9. The activity of the three nanozymes is low in acidic solution, and the catalytic activity is the highest at near neutral (pH 8.0), which is different from the optimal catalytic pH (3.5–5.0) of peroxide-like nanozymes reported previously. This unique behavior can be attributed to several synergistic factors rooted in the material's composition and dual-enzyme characteristics. First, the specific coordination environment of Fe^{3+} within the Fe-His framework modulates the electronic properties of the hemin center and histidine residues, stabilizing the active site and extending its operational pH range into slightly alkaline conditions. At pH 8.0, key functional groups (*e.g.*, the imidazole of histidine) are in

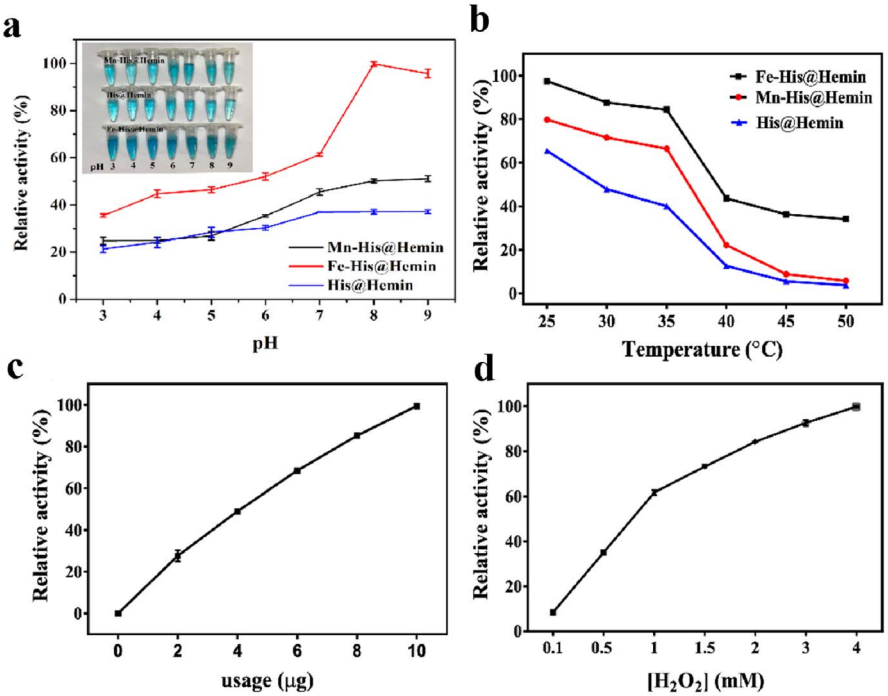

Fig. 4 The influence of different reaction conditions on peroxidase-like activity of Fe-His@Hemin. Effect of (a) pH and (b) temperature on the activity of Fe-His@Hemin, Mn-His@Hemin, His@Hemin; (c) effect of catalyst dosage on the activity of Fe-His@Hemin + H_2O_2 + TMB system; (d) effect of H_2O_2 concentration on the activity of Fe-His@Hemin + H_2O_2 +TMB system. The error bars are the standard deviation of the third parallel sample.

a deprotonated state, which enhances their electron-donating ability to the Fe^{3+} center, thereby promoting substrate (H_2O_2 and TMB) binding and catalytic turnover. Second, the inherent CAT-like activity of Fe-His@Hemin plays a crucial synergistic role at this pH. The CAT-like activity converts a portion of the H_2O_2 back to O_2. This *in situ* regenerated O_2 can be instantly reused by GOx in detection assays, accelerating the overall reaction flux and thereby ensuring a high net production rate of H_2O_2 for the peroxidase-like (POD-like) cycle.

Thus, the concurrent enhancement of both POD-like and CAT-like activities at pH 8.0, driven by the favorable coordination chemistry and reaction dynamics, underpins the superior catalytic performance of Fe-His@Hemin under physiological-relevant conditions.

Fig. 4b demonstrates that within the temperature range, the catalytic activity of the three nanozymes decreased with the increase of temperature. Fe-His@Hemin has a good catalytic activity of more than 80% at 25–35 °C. According to the investigation results, Fe-His@Hemin was selected as the follow-up experimental investigation material. The catalytic activity of nanozyme increases with the increase of nanozyme concentration. Based on maintaining solubility and stability, the optimal concentration is selected as 6 μg mL^{-1} (Fig. 4c). Fig. 4d investigates the effect of H_2O_2 concentration on the catalytic activity. The activity increases with H_2O_2 concentration up to a certain point, after which it plateaus or slightly decreases due to potential substrate inhibition. As a result, the optimum catalytic conditions for: pH 8.0, temperature 25 °C, catalyst concentration 6 μg mL^{-1}.

3.3. Catalase-like activity Fe-His@Hemin and double enzyme activity catalytic mechanism

In addition, we found that in the alkaline catalytic environment at room temperature, small but dense bubbles appeared in the reaction solution, indicating that Fe-His@Hemin could catalyze H_2O_2 to produce O_2, confirming its CAT-like property. The experimental results are shown in Fig. S4. Within the pH range investigated, the bubbles of the reaction solution increased with the increase of pH. When pH was 8.0, the bubbles produced by the centrifugal tube were the most. Fe-His@Hemin shows highest activity at pH 8.0. This unique pH profile is attributed to the synergistic effect of its dual-enzyme activities (POD-like and CAT-like), which are both enhanced at this pH (Fig. 4a). Then, we compared the amount of oxygen produced by Fe-His@Hemin with that produced by His@Hemin using a dissolved oxygen analyzer (Fig. S4b).Under the same reaction condition, the oxygen produced by Fe-His@Hemin was twice that by His@Hemin, indicating that the addition of iron significantly enhanced the CAT activity of the nanozyme.The dual-enzyme characteristics of Fe-His@Hemin can be explained by the specific coordination environment of the Fe^{3+} ions within the nanozyme structure. The presence of Fe^{3+} creates a unique electronic environment that modulates the electronic properties of the hemin and histidine residues, facilitating catalytic

activities at a broader pH range, including slightly alkaline conditions. At pH 8.0, the CAT-like activity generates O_2. In a detection cascade involving GOx, this *in situ* generated O_2 is recycled to drive the oxidation of glucose, thereby accelerating the net production of H_2O_2, which in turn supplies the POD-like activity. This synergistic effect results in higher overall catalytic efficiency compared to acidic conditions. The dual-enzyme characteristics of Fe-His@Hemin create a synergistic cycle in the glucose detection cascade, rather than a simple competition for H_2O_2. The intended mechanism is as follows: in the one-step assay, GOx first oxidizes glucose, consuming dissolved O_2 and generating H_2O_2. The CAT-like activity of Fe-His@Hemin then comes into play not by producing H_2O_2, but by converting a portion of this enzymatically generated H_2O_2 back into O_2 and H_2O. This *in situ* regenerated O_2 is immediately available for the GOx reaction, effectively creating an intrinsic O_2-recycling loop.This loop is crucial because it addresses a common limitation in oxidase-based detection systems: the depletion of dissolved O_2, which can slow down the GOx reaction. By recycling O_2 from the H_2O_2 intermediate, the CAT-like activity prevents O_2 from becoming a limiting factor, thereby accelerating the net production rate of H_2O_2 by GOx. Consequently, the overall flux of the cascade is increased. The POD-like activity, operating in parallel, then utilizes this efficiently and continuously generated H_2O_2 pool to oxidize TMB, producing the colorimetric readout. Thus, the CAT-like and POD-like activities function synergistically: the former drives the substrate (O_2) regeneration to fuel the H_2O_2-producing step, while the latter efficiently converts the accumulated H_2O_2 into a detectable signal.

To explore the catalytic mechanism of Fe-His@Hemin with double enzyme activities, the effects of different free radical trapping agents on the reaction system were selected, and the types of reactive oxygen species (ROS) generated during the catalytic process were studied. Different concentrations of *p*-benzoquinone, NaN_3 and thiourea were used as trapping agents for $O_2^{\bullet-}$, $^1O_2$, and $^{\bullet}OH$, respectively.[30–32] The experimental results showed that the addition of three trapping agents to the reaction system inhibited the color development of the system, indicating that there were three ROS ($O_2^{\bullet-}$, $^1O_2$, and $^{\bullet}OH$) in the system, and thiourea had obvious inhibition effect in the same concentration of trapping agents, indicating that the main ROS species in the system was $^{\bullet}OH$ (Fig. S5). Therefore, based on the above results, it can be inferred that the catalytic mechanism of Fe-His@Hemin in a neutral solution with pH 8.0 is as follows: under neutral conditions, Fe-His@Hemin can catalyze H_2O_2 to produce $^{\bullet}OH$ in the system, which shows the catalytic properties of Fe-His@Hemin POD-like enzymes. At the same time, because Fe-His@Hemin has the property of CAT-like, H_2O_2 in the system can be decomposed into O_2, and the generation of *in situ* O_2 can further produce ROS.

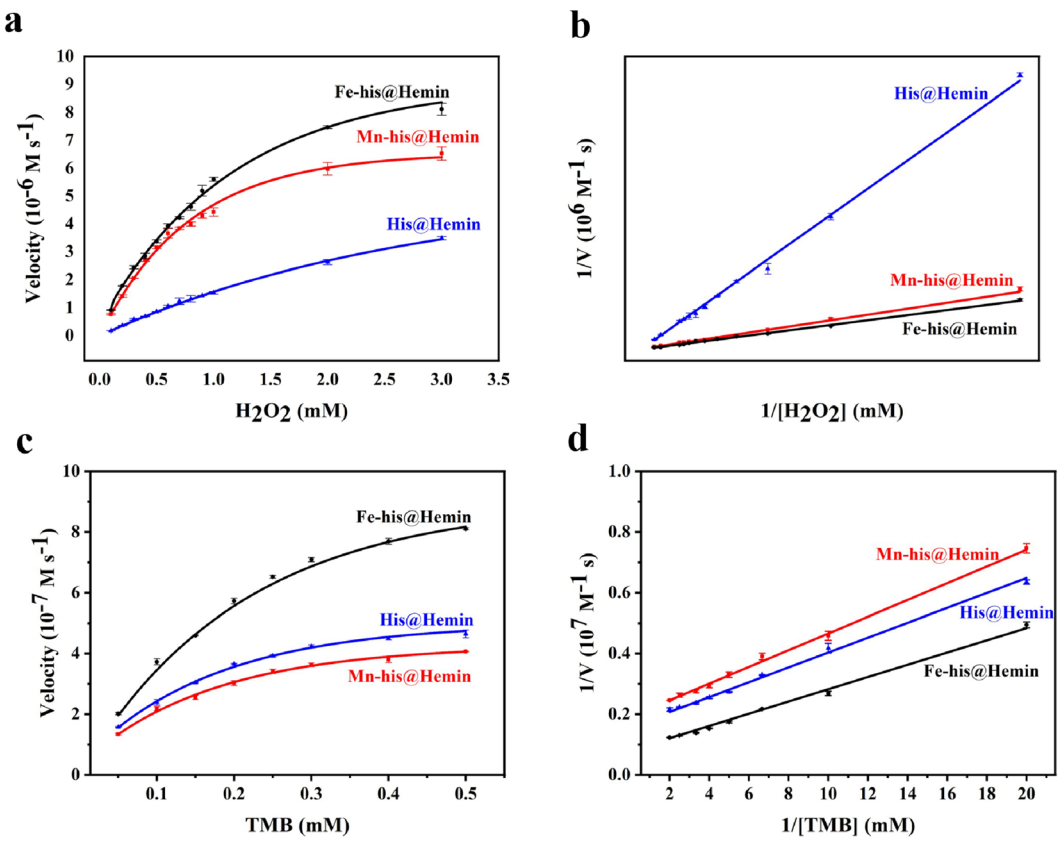

Fig. 5 Kinetic studies of the POD-like experiment of Fe-His@Hemin, Mn-His@Hemin, His@Hemin. (a) 0.3 mM TMB with different concentrations of H_2O_2. (c) 1 mM H_2O_2 with different concentrations of TMB. (b) and (d) Double reciprocal of (a) and (c), respectively. The error bars are the standard deviation of the third parallel sample.

3.4. Kinetic analysis and reaction mechanism of Fe-His@Hemin

Subsequently, steady-state kinetic experiments were performed for the further evaluation of peroxidase-like properties for Fe-His@Hemin, Mn-His@Hemin and His@Hemin. After being fitted by Lineweaver–Burk plots (Fig. 5), the Michaelis–Menten constant (K_m) and maximum initial velocity (V_{max}), two important parameters in enzyme catalysis, are summarized in Table S1 (see SI). Lower K_m values always reveal that the proposed nanozymes have a much higher affinity to the corresponding substrate. Notably, Fe-His@Hemin exhibits a significantly lower K_m for H_2O_2 compared to many reported nanozymes, indicating a substantially higher affinity for this primary substrate. This value is also lower than that of natural HRP (3.7 mM), underscoring the efficient substrate binding facilitated by the unique Fe^{3+} coordination environment in our material. Furthermore, the calculated V_{max} for Fe-His@Hemin is among the highest listed, demonstrating its superior catalytic turnover capability. The combination of a low K_m (high affinity) and a high V_{max} clearly substantiates the claim that Fe-His@Hemin possesses distinct advantages, particularly in terms of catalytic efficiency and substrate affinity under neutral conditions, over a range of previously developed peroxidase-mimicking nanomaterials. The results in Fig. 5 showed that compared with Mn-His@Hemin and His@Hemin, Fe-His@Hemin has a smaller K_m and the higher V_{max}. With H_2O_2 as the substrate, K_m of Fe-His@Hemin is only one fifth of that of His@Hemin. For TMB as substrate, the V_{max} of Fe-His@Hemin is about twice that of Mn-His@Hemin and His@Hemin, indicating that the hemin after the addition of iron improves the affinity of substrate H_2O_2 and the catalytic activity of enzymes. Thus, Fe-His@Hemin has enhanced peroxidase-like activity, which can be attributed to its unique Fe^{3+} coordination geometry and its well-dispersed spherical morphology in aqueous solution. Compared with the previously reported peroxide-like nanomaterials, the material Fe-His@Hemin has obvious advantages and has good application prospects in practical catalysis.

3.5. Detection of H_2O_2 and glucose using the Fe-His@Hemin

The detection of H_2O_2 is essential in many fields such as life activities, medical diagnosis, industrial and agricultural production and environmental monitoring. Therefore, it is of great significance to establish a simple, fast, highly sensitive and visual detection of H_2O_2 without any complex instruments. The colorimetric sensor of H_2O_2 was established under the best conditions by utilizing the double enzyme properties of Fe-His@Hemin. The UV-vis spectral curve of H_2O_2 (0.25–120 μM) at 652 nm was detected in Fig. S6. With the increase of H_2O_2 concentration in the system Fe-His@Hemin-TMB, the absorbance value A also increases continuously ($A = A - A_0$, A and A_0 refer to the absorption value of H_2O_2 at 652 nm in the system with and without H_2O_2, respectively), and there is A good linear relationship between A and H_2O_2 in the range of 0.25–120 μM

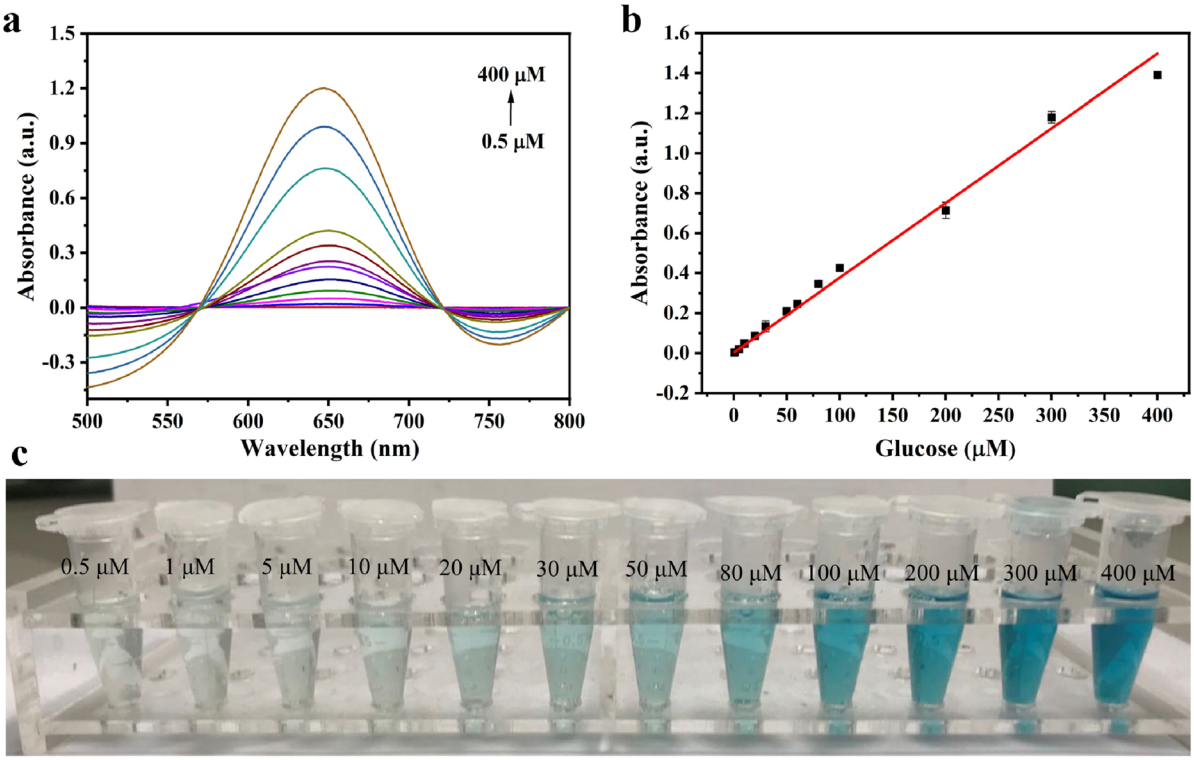

Fig. 6 Sensitivity research of glucose colorimetric sensing platform based on Fe-His@Hemin. (a) The spectra of the sensing system with different glucose concentrations; (b) the linear relationship between absorbance (A) and glucose concentrations from 0.5–400 μM; (c) photographs of the colorimetric response to different glucose concentrations (0.5–400 μM). The error bars are the standard deviation of the third parallel sample.

(Fig. S6b). The linear equation is $\Delta A = 0.00582\ [H_2O_2]\ (\mu M) + 0.01601$ ($R^2 = 0.99879$). The detection limit was 0.16 μM. According to the $3\sigma/k$ rule, the detection limit of H_2O_2 is 0.16 μM. Compared with other colorimetric methods for the detection of H_2O_2 (Table S2), the colorimetric method adopted in this study has higher sensitivity and lower detection limits.

In the actual clinical test, the glucose content in the blood and urine is an important indicator of the diagnosis of human health. Most of the reported nanozymes used the activity of POD-like simulated enzymes to establish glucose colorimetric biosensors under acidic conditions (pH 3.5–4.5). The detection mechanism is as follows: first, glucose oxidase can quantitatively catalyze glucose to produce H_2O_2; subsequently, under the action of nanozyme, H_2O_2 catalyzes the color development of the substrate leading to changes in the system solution (steps 1 and 2). However, the optimal catalytic pH of glucose oxidase is neutral, and the peroxidase activity of most nanozymes often shows the best catalytic performance under acidic conditions. Therefore, the simple and rapid quantitative detection of glucose has practical significance in potential biomedical applications.

$$C_6H_{12}O_6(\text{glucose}) + O_2 + H_2O \xrightarrow{GO_x} C_6H_{12}O_7(\text{gluconic acid}) + H_2O_2 \quad (1)$$

$$AH + H_2O_2 \xrightarrow{\text{peroxidase}} 2A + H_2O \quad (2)$$

Based on the advantages of self-replenishing oxygen in Fe-His@Hemin systems with good POD-like and CAT-like activities under neutral conditions, we established a one-step efficient visual glucose biosensor. The experimental results are shown in Fig. 6, the result shows the ultraviolet-visible spectral curve of glucose (0.5–400 μM) detected at 652 nm. As the concentration of glucose increases, the absorbance of the solution gradually increases. The Glucose concentration showed an excellent linear correlation ($R^2 = 0.9949$)between 0.5 μM and 400 μM (Fig. 6b), and the linear regression equation was $A = 0.00374$ [Glucose] (μM) + $0.0035C$ ($R^2 = 0.9949$). Fig. 6c visually demonstrates the color gradient corresponding to the glucose concentration range. The concentration of glucose in the sample can be directly and quickly judged by the intensity of the color of the solution. According to the $3\sigma/k$ rule, the glucose detection limit (LOD) is 0.25 μM. Compared with most reported glucose detection sensors (Table S3), the method reported in this paper has a wider linear range, high sensitivity, and low detection limit, which can have a good prospect in clinical diagnosis.

3.6. Application of the glucose sensor

Fe-His@Hemin stability was evaluated by measuring relative activity every 5 days at 1 month of storage at room temperature. The experimental results are shown in Fig. 7a. The catalytic activity of Fe-His@Hemin remains above 90%, which proves that the nanomaterial has good stability. In addition, to verify

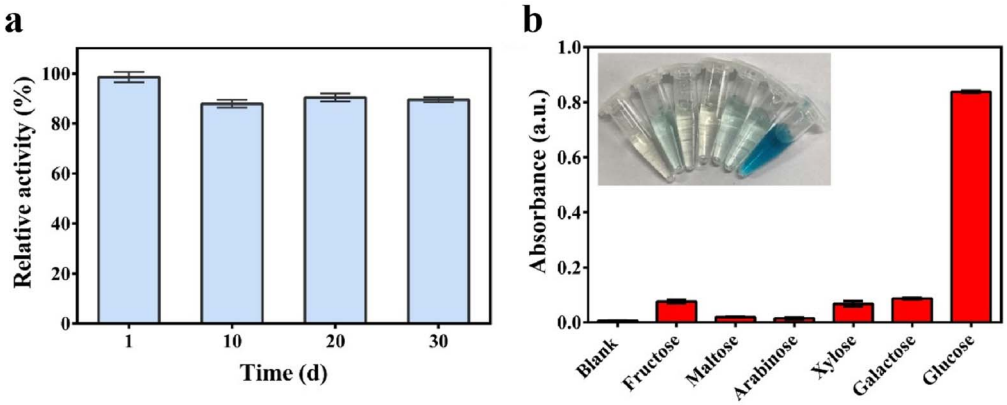

Fig. 7 The stability of Fe-His@Hemin. (a) The long-term stability of Fe-His@Hemin; (b) the selectivity analysis for glucose detection with different sugars (0.4 mM glucose, 4 mM fructose, maltose, arabinose, xylose, galactose; (Inset) the picture of the corresponding samples). The error bars are the standard deviation of the third parallel sample.

Table 1 Determination results of glucose in human serum samples

Sample	Found in sample (μM)	Spiked (μM)	Found±SD (μM)	Recovery (%)	RSD (%)
1	36.89	100.00	136.35 ± 1.28	98.2	1.3
		200.00	237.73 ± 1.84	101.9	1.8
		300.00	336.91 ± 2.99	99.76	2.7
2	33.29	100.00	132.85 ± 1.13	99.5	1.1
		200.00	233.87 ± 2.28	102.6	1.5
		300.00	331.91 ± 3.14	96.7	1.9

that the sensor established in this paper has good selectivity for glucose, we selected fructose (4 mM), maltose (4 mM), arabinose (4 mM), xylose (4 mM), galactose (4 mM) and glucose (0.4 mM) for comparison. As shown in Fig. 7b, the solutions with high concentrations of fructose, maltose, arabinose, xylose, and galactose showed no obvious color changes, while the solutions with only 0.4 mM of glucose were significantly bluer. The results show that the colorimetric sensor has high selectivity for glucose and can be further applied in biomedicine, biological detection and biotechnology.

According to the American Diabetes Association and WHO criteria, the clinical cut-off for random (non-fasting) blood glucose is 11.1 mmol L^{-1} ($\approx$200 mg dL^{-1}) for diabetes diagnosis and 7.8 mmol L^{-1} ($\approx$140 mg dL^{-1}) for impaired glucose tolerance. In healthy individuals, fasting plasma glucose is <6.1 mmol L^{-1} ($\approx$110 mg dL^{-1}). Because our colorimetric signal plateaus when glucose $\geq$400 μM, the response deviates from linearity beyond this point. When undiluted human serum samples (original glucose $\approx$5–7 mmol L^{-1}) were assayed after a 50-fold dilution, the measured concentration after dilution fell between 100–140 μM, well within the linear range (0.5–400 μM). Therefore, the upper limit of 400 μM does not compromise quantification in routine clinical use. After the recommended 50-fold dilution, the expected glucose concentration in diluted serum is 100–140 μM, which lies comfortably inside the validated linear window. Recovery tests at three spiking levels (100, 200, 300 μM) yielded 96.7–102.6% with RSD <2.7% (Table 1), confirming that the 0.5–400 μM range is appropriate for accurate glucose quantification in human serum with the described dilution protocol.

4 Conclusion

In summary, a novel bionic nanomaterial with double enzyme properties Fe-His@Hemin has been prepared in this paper. Because of the synergistic action of peroxidase and catalase, Fe-His@Hemin has achieved high efficiency in the catalytic process of TMB. Compared with HRP enzyme, Fe-His@Hemin has higher affinity for H_2O_2 and TMB substrates. At the same time, we constructed a colorimetric sensor for H_2O_2 and glucose. The linear ranges of H_2O_2 and glucose were 0.25–120 μM and 0.5–400 μM, respectively, and the detection limits were 0.16 μM and 0.25 μM, respectively. The sensor has high sensitivity and selectivity, good recovery rate, and can be used in future biological analysis and clinical diagnosis.

Ethical statement

The human serum used in this study was sourced from the blood bank of the First Affiliated Hospital of Jilin University. All experiments were performed in accordance with the Guidelines "Declaration of Helsinki (as revised in 2013)", and approved by the ethics committee at "the Institutional Ethics Committee of the First Affiliated Hospital of Jilin University". Informed consents were obtained from human participants of this study.

Author contributions

Conceptualization: Y. L.; methodology: Y. W., Y. G., X. F.; formal analysis and investigation Y. W., Y. G., X. F.; writing—original draft preparation: Y. L.; writing—review and editing: Y. L., A. W., Y. M.; funding acquisition: Y. L.; supervision: Y. J., X. L. All authors reviewed the manuscript.

Conflicts of interest

The authors declare no competing interests.

Data availability

Data is provided within the manuscript or supplementary information (SI) files. Supplementary information is available. See DOI: https://doi.org/10.1039/d6ra00649c.

Acknowledgements

This work was financially stabilized by the National Natural Science Foundation of Henan Province (242300421514), Independent research project of the Central China Branch of the National Center for Cardiovascular Diseases (2024-FZX11), Young Elite Scientists Sponsorship Program by Henan Association for Science and Technology (2025HYTP078), and Henan Province Key R&D Program (232102310292).

References

1 M. Garcia-Viloca, J. Gao, M. Karplus, *et al.*, How enzymes work: Analysis by modern rate theory and computer simulations, *Science*, 2004, **303**(5655), 186–195.
2 S. He, L. Ma, Q. Zheng, Z. Wang, W. Chen, Z. Yu, X. Yan and K. Fan, Peptide nanozymes: An emerging direction for functional enzyme mimics, *Bioact. Mater.*, 2024, **42**, 284–298.
3 Y. An, X. Fang, J. Cheng, S. Yang, Z. Chen and Y. Tong, Research progress of metal-organic framework nanozymes in bacterial sensing, detection, and treatment, *RSC Med. Chem.*, 2023, **15**(2), 380–398.
4 R. Zhang, K. Fan and X. Yan, Nanozymes: created by learning from nature, *Sci. China Life Sci.*, 2020, **63**(8), 1183–1200.
5 U. Markel, D. F. Sauer, M. Wittwer, *et al.*, Chemogenetic Evolution of a Peroxidase-like Artificial Metalloenzyme, *ACS Catal.*, 2021, **11**(9), 5079–5087.
6 X. Mou, Q. Wu, Z. Zhang, Y. Liu, J. Zhang, C. Zhang, X. Chen, K. Fan and H. Liu, Nanozymes for Regenerative Medicine, *Small Methods*, 2022, **6**(11), e2200997.
7 J. Sheng, Y. Wu, H. Ding, K. Feng, Y. Shen, Y. Zhang and N. Gu, Multienzyme-Like Nanozymes: Regulation, Rational Design, and Application, *Adv. Mater.*, 2024, **36**(10), e2211210.
8 Y. Yang, D. M. Zhu, Y. Liu, *et al.*, Platinum-carbon-integrated nanozymes for enhanced tumor photodynamic and photothermal therapy, *Nanoscale*, 2020, **12**(25), 13548–13557.
9 N. Losada-Garcia, A. Jimenez-Alesanco, A. Velazquez-Campoy, O. Abian and J. M. Palomo, Enzyme/Nanocopper Hybrid Nanozymes: Modulating Enzyme-like Activity by the

Protein Structure for Biosensing and Tumor Catalytic Therapy, *ACS Appl. Mater. Interfaces*, 2021, **13**(4), 5111–5124.

10 Y. Ouyang, M. P. O'Hagan and I. Willner, Functional catalytic nanoparticles (nanozymes) for sensing, *Biosens. Bioelectron.*, 2022, **218**, 114768.

11 C. Wu, Q. Li, R. Su, Y. Wang and W. Qi, Construction of Smartphone-Integrated Nanozyme Sensor Based on Amino Acid-Modulated Gold Nanoparticles, *Chembiochem*, 2024, **25**(17), e202400370.

12 X. Zhang, Y. Wang, Y. Dai and F. Xia, Tuning the enzyme-like activity of peptide-nanoparticle conjugates with amino acid sequences, *Nanoscale*, 2023, **15**(18), 8148–8152.

13 S. Sun, Z. Zhang, Y. Xiang, M. Cao and D. Yu, Amino Acid-Mediated Synthesis of the ZIF-8 Nanozyme That Reproduces Both the Zinc-Coordinated Active Center and Hydrophobic Pocket of Natural Carbonic Anhydrase, *Langmuir*, 2022, **38**(4), 1621–1630.

14 L. Tu, S. Chen, Z. Yuan, Y. Xiong, B. Luo, Y. Chen, Z. Hou, S. Ke, N. Lin, C. Li and S. Ye, Amino acid-based metallo-supramolecular nanoassemblies capable of regulating cellular redox homeostasis for tumoricidal chemo-/photo-/catalytic combination therapy, *J. Colloid Interface Sci.*, 2024, **663**, 810–824.

15 S.-Y. Chiang, C.-H. Peng, J.-W. Lin, J.-W. Kuo, Y.-W. Lin, C.-H. Lin and C.-Y. Chen, Amino-Acid-Engineered Bionanozyme Selectivity for Colorimetric Detection of Human Serum Albumin, *ACS Appl. Mater. Interfaces*, 2025, **17**(14), 20693–20704.

16 N. Zhu, C. Liu, R. Liu, X. Niu, D. Xiong, K. Wang, D. Yin and Z. Zhang, Biomimic Nanozymes with Tunable Peroxidase-like Activity Based on the Confinement Effect of Metal-Organic Frameworks (MOFs) for Biosensing, *Anal. Chem.*, 2022, **94**(11), 4821–4830.

17 B. Xu, H. Wang, W. Wang, L. Gao, S. Li, X. Pan, H. Wang, H. Yang, X. Meng, Q. Wu, L. Zheng, S. Chen, X. Shi, K. Fan, X. Yan and H. Liu, A Single-Atom Nanozyme for Wound Antibacterial Applications, *Angew. Chem., Int. Ed.*, 2019, **58**(15), 4911–4916.

18 H. Sun, Y. Zhou, J. Ren, *et al.*, Carbon Nanozymes: Enzymatic Properties,Catalytic Mechanism, and Applications, *Angew. Chem., Int. Ed.*, 2018, **57**(30), 9224–9237.

19 Y. Luo, H. Luo, S. Zou, J. Jiang, D. Duan, L. Chen and L. Gao, An In Situ Study on Nanozyme Performance to Optimize Nanozyme-Strip for Aβ Detection, *Sensors*, 2023, **23**(7), 3414.

20 F. Wei and X. J. Han, Nanozymes and Their Application Progress in Biomedical Detection, *Chin. J. Anal. Chem.*, 2021, **49**(4), 581–592.

21 X. Hu, G. Wang, K. Fang, R. Li, C. Dong, S. Shi and H. Li, The construction of Fe-porphyrin nanozymes with peroxidase-like activity for colorimetric detection of glucose, *Anal. Biochem.*, 2023, **675**, 115224.

22 X. Li, X. Yang, X. Cheng, *et al.*, Highly dispersed Pt nanoparticles on ultrasmall EMT zeolite: A peroxidase-mimic nanoenzyme for detection of H_2O_2 or glucose, *J. Colloid Interface Sci.*, 2020, 570300–570311.

23 R. Xu, X. Tan, T. Li, S. Liu, Y. Li and H. Li, Norepinephrine-induced AuPd aerogels with peroxidase- and glucose oxidase-like activity for colorimetric determination of glucose, *Mikrochim. Acta*, 2021, **188**(11), 362.

24 W. Zhang, X. Li, T. Cui, S. Li, Y. Qian, Y. Yue, W. Zhong, B. Xu and W. Yue, PtS_2 nanosheets as a peroxidase-mimicking nanozyme for colorimetric determination of hydrogen peroxide and glucose, *Mikrochim. Acta*, 2021, **188**(5), 174.

25 Q. Wang, X. Zhang, L. Huang, Z. Zhang and S. Dong, One-Pot Synthesis of Fe_3O_4 Nanoparticle Loaded 3D Porous Graphene Nanocomposites with Enhanced Nanozyme Activity for Glucose Detection, *ACS Appl. Mater. Interfaces*, 2017, **9**(8), 7465–7471.

26 L. Su, Y. Cai, L. Wang, W. Dong, G. Mao, Y. Li, M. Zhao, Y. Ma and H. Zhang, Hemin@carbon dot hybrid nanozymes with peroxidase mimicking properties for dual (colorimetric and fluorometric) sensing of hydrogen peroxide, glucose and xanthine, *Mikrochim. Acta*, 2020, **187**(2), 132.

27 Y. Huang, Z. Ding, Y. Li, F. Xi and J. Liu, Magnetic Nanozyme Based on Loading Nitrogen-Doped Carbon Dots on Mesoporous Fe_3O_4 Nanoparticles for the Colorimetric Detection of Glucose, *Molecules*, 2023, **28**(12), 4573.

28 S. Fu, J. Liu, S. Wu, *et al.*, Gold nanoparticle-loaded MoS_2 nanosheets with peroxidase-like and pyranose oxidase-like activities for bio-enzyme-free visual detection of glucose, xylose and galactose, *Mater. Adv.*, 2024, **5**(10), 10.

29 M. Aghayan, A. Mahmoudi, K. Nazari, *et al.*, Fe (III) porphyrin metal-organic framework as an artificial enzyme mimics and its application in biosensing of glucose and H_2O_2, *J. Porous Mater.*, 2019, **26**(5), 1507–1521.

30 L. J. Chen, H. Y. Gao, Y. Bai, W. Wei, J. F. Wang, G. E. Fakhri and M. Y. Wang, Colorimetric biosensing of glucose in human serum based on the intrinsic oxidase activity of hollow MnO_2 nanoparticles, *New J. Chem.*, 2020, **44**, 15066–15070.

31 M. Bancirova, Sodium azide as a specifc quencher of singlet oxygen during chemiluminescent detection by luminol and Cypridina luciferin analogues, *Luminescence*, 2011, **26**, 685–688.

32 I. Gültekin, G. Tezcanli-Güyer and N. H. Ince, Sonochemical decay of C.I. Acid Orange 8: efects of CCl4 and t-butyl alcohol, *Ultrason. Sonochem.*, 2009, **16**, 577–581.